Extensive Air Shower Reconstruction using the timing information from the RF-system of the Astroneu array

S Nonis[2], A Leisos[1], A Tsirigotis[1], G Bourlis[1], K Papageorgiou[2], I Gkialas[2], I Manthos[3] and S Tzamarias[3]

[1] Physics Laboratory, School of Science and Technology, Hellenic Open University, Patras 26222, Greece
[2] School of Engineering, Department of Financial and Management Engineering, University of the Aegean, Chios 82100, Greece
[3] Department of Physics, Aristotle University of Thessaloniki, Thessaloniki 54124, Greece

E-mail: snonis@aegean.gr

Abstract. The Astroneu cosmic ray telescope is a distributed hybrid array consisting of both scintillator counters and RF antenna detectors used for the detection of extensive air showers (EAS). The array is deployed at the Hellenic Open University campus, on the outskirts of the urban area of Patras in Greece. In the present development phase, the Astroneu telescope includes two stations consisting of 3 scintillation detectors modules (SDM) and one RF antenna while a third station includes 3 particle detectors and 4 RF antennas (3SDM-4RF). In each station, the RF-detectors are operating receiving a common trigger upon a 3-fold coincidence between the particle detectors of the station. In this study we present recent results from the 3SDM-4RF autonomous station related to the estimation of the direction of the incoming cosmic air shower using only the timing information from the 4 RF detectors. The directions of the reconstructed showers using the RF timing are in agreement with the corresponding results using the SDMs timing as well as with the simulation predictions. This verifies that the RF signal emitted from EAS originating form Ultra High Energy Cosmic Rays (UHECR), can be detected even in areas with strong electromagnetic background.

Keywords: Cosmic rays, Astroneu, radio detection of extensive air showers, RF timing.

1. Introduction

The term cosmic rays (CR) refers to energetic atomic nuclei with extra terrestrial origin. At energies above 100 TeV the direct detection of cosmic rays with balloons or satellites is significantly reduced due to the low flux, while beyond these energies the detection of secondary particles generated by the interaction of the primary particle with air nuclei (called extensive air shower - EAS), is a commonly used detection method. During the shower development in the atmosphere, different emissions of electromagnetic radiation occurs in both the optical (Cherenkov radiation or fluorescence emission) and radio frequency range (RF emission) [1]. For EAS generated from cosmic particles with energies grater than 100 PeV the RF signal is detectable at the ground level as verified by a series of experiments over the last twenty years [2, 3, 4, 5, 6]. The RF signal observations are usually carried out in the frequency range 30-80

MHz, while depending on the bandwidth of the antenna used, is possible to extend observations in higher or lower frequencies [7, 8].

The great progress that the RF signal detection technique has made in the last years is demonstrated by the fact that the main parameters of the primary cosmic ray (type, energy, arrival direction) can be reconstructed with an accuracy approaching that of more traditional techniques (particle detectors or fluorescence telescopes). In addition, recent studies show that both the energy [9] and the arrival direction [10] of the primary particle can be estimated even from the power spectrum of a single antenna. The RF signal detection has a duty cycle approximately 100% (except during thunderstorms) while the limited cost of the RF stations allows the coverage of larger areas [1] for the study of high energy cosmic rays and neutrinos i.e. the future GRAND experiment [11] with 200,000 antennas over an area of 200,000 km^2.

The RF signal emitted from an EAS is produced from two main mechanisms. The more dominant is the time variation of a current perpendicular to the shower axis, which is created by the deflection of EAS electrons and positrons in the geomagnetic field [12]. The generated field by the geomagnetic mechanism is expected to be linearly polarized in the direction of $\boldsymbol{v}_{(\boldsymbol{e}^-/\boldsymbol{e}^+)} \times \boldsymbol{B}_{\boldsymbol{geo}}$. The second mechanism that contributes to the RF emission emerges from the excess of electrons at the shower front [13] which develops a time depended current in the shower's axis direction. The polarization of the created electric field, in this case, is vertical to shower's axis.

The Astroneu cosmic ray telescope is a small scale hybrid array located at the Hellenic Open University (HOU) campus near the city of Patras in Greece. In previous studies, the performance of the Astroneu array was demonstrated emphasizing on the detection and reconstruction of EAS using the particle detectors of the array [14, 15]. The detection of the RF signals from EAS, in areas with strong electromagnetic noise, was achieved by imposing appropriate selection criteria to the RF signals [16]. Studies concerning the timing and the amplitude strength of the RF signals were performed by comparing the RF data with the SDM data, as well as with simulation predictions [17]. Furthermore a complete Voltage Response Model (VRM) for the RF system was established using the antenna's Vector Effective Length (VEL) and the measured RF spectra at the antenna's position for estimating the shower's axis direction [10, 18].

In the present work recent results are presented demonstrating the estimation of the shower's axis direction using only the timing information from the RF detectors. In addition a Monte Carlo (MC) simulation analysis was carried out for evaluating the performance of the method. The reconstructed EAS directions as emerged from the RF timing data are compared with the results of an independent shower axis reconstruction using the particle detector as well as the results of simulation studies.

The paper is organized as follows: In Section 2 the detectors and performance of the Astroneu array is reported, while in Section 3 the simulation sample and the method for reconstructing the direction of the EAS using the RF timing is presented. In Section 4 the comparison of the RF data with the simulation sample is presented, while in Section 5 the direction reconstruction using the RF data is compared with the corresponding reconstruction using the particle detector data. Finally, Section 6 summarizes the conclusions.

2. The Astroneu array

Astroneu is a small scale EAS detection array comprising 9 scintillator detectors and 6 RF antennas, arranged in three autonomous stations (A, B and C). In its present development state stations B and C include 3 Scintillator Detector Modules (SDM) [14] and one RF antenna [19] (3SDM-1RF) while at station A the 3 SDMs are surrounded by 4 antennas (3SDM-4RF) [22] (figure 1-left). Each station is equipped with electronics for triggering, digitization and Data

[1] Compared with the areas covered by particle detectors in existing experiments.

Acquisition (DAQ) together with slow control and monitor electronics and a GPS-based timing system.

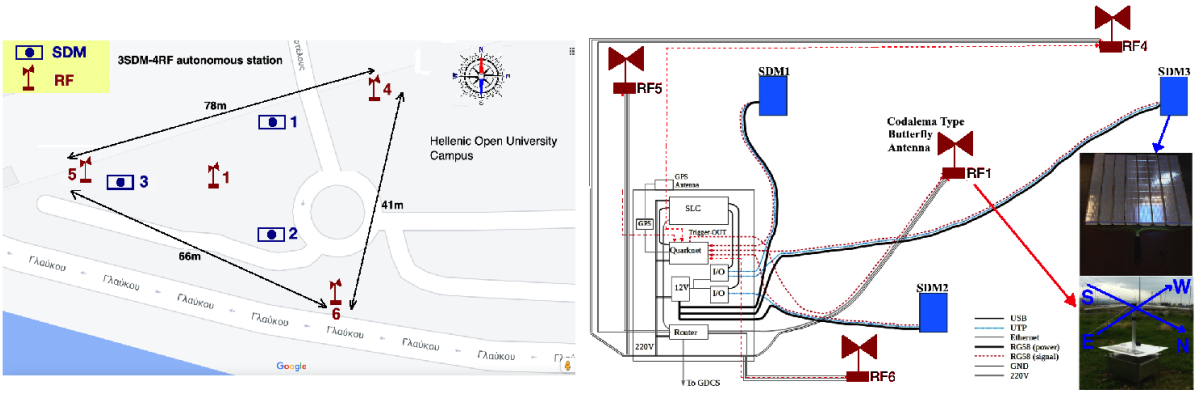

Figure 1. (*Left*) The layout of Astronue's 3SDM-4RF [22] station. The 3 SDMs are marked with blue squares, while the 4 RF antennas with red bow ties. (*Right*) Schematic description of the connections in the 3SDM-4RF station.

The SDM incorporates 160 scintillating tiles in an area of 1 m^2. The light emitted due to the interaction of the shower particles with the scintillation material is collected and led to a single Photomultiplier tube (PMT) using 96 embedded wavelength shifting fibers (WLS). The RF system consists of two bow tie shaped dipoles which are oriented in the directions of East-West (EW) and North-South (NS). At the top of the arm that holds the two dipoles is placed a Low Noise Amplifier (LNA) to which the signals from both directions are amplified. The RF system is designed and implemented by the Codalema collaboration [19]. The RF system is accompanied by electronic modules for triggering, digitization and event time-stamping (GPS card). When all 3 SDMs of the station acquired signals above a predetermined threshold an external trigger activates the signal recording in the RF system and the waveforms of the two dipoles were sampled at a rate of 1GHz. A schematic representation of the Astroneu station-A connections is shown in figure 1 (right).

A Quarknet electronics board [23] is used for the collection of the 3 SDMs signals as well as for the digitization of the crossing of the waveforms with a predefined voltage threshold. The first crossing is used for timestamping while the amount of time that the pulse stays beyond the threshold (Time over Threshold-ToT) is used for the estimation of the pulse size [15]. Absolute synchronization is provided by a GPS receiver. The station's I/O and network devices, the Quarknet board as well as the Station Local Computer (SLC) are placed inside a metallic Central Electronics Box (CEB). Upon a trigger, the recording of the EW and NS waveforms of the RF antennas are initiated. The signals are digitized by an ADC (1GS/s over 2560 points for 2.56 μs record) and timestamped using the RF system GPS. The experimental data from both the SDMs and the antennas of the station are stored to the Global Data and Control Server (GDCS), where the event is retrieved offline using the GPS time-tags.

The 3SDM-4RF [22] station of the Astroneu array has the ability to reconstruct EAS of energy more than 10 TeV with a typical resolution of 3.5 degrees at a rate of 17.5 h^{-1}. The efficiency of the Astroneu array in detecting and reconstructing EAS using the data from the SDMs of one station (single station operation) or by combining the data information from two stations (multiple station operation) is reported in [20, 21].

3. Simulation Studies

For the simulation studies a sample of Monte Carlo shower events was generated through a three-step process. In the first stage EAS with energy ranged between 1 PeV and 2 EeV (corresponding to 348,000 hours of experimental time) were produced with the CORSIKA simulation package [26]. For the high energy hadronic interactions the packages QGSJET-II-04 [24] was employed while the EGS4 code [27] was used for the simulation of the electromagnetic interactions. The type of the primary nuclei and the spectral index were selected according to measurements described in [25]. The simulations EAS directions covered a wide range of zenith ($0^o \leq \theta \leq 60^o$) and azimuth ($0 \leq \phi \leq 360^o$) angles while the showers impact point in the ground were selected inside a circle of radius 400 m around the station's center.

In the second simulation stage the RF signal generation was realized with the SELFAS [28] simulation software. The electric field, as calculated from SELFAS in the antennas positions, was convoluted [2] with the RF system's (antenna+LNA) VEL for calculating the voltage induced in the antennas dipole (analytic description for the RF signal convolution with VEL can be found in [10, 18]). In the final simulation stage the RF signal was distorted according to the background noise of the area as estimated from a large number of noise events [3] ($>10^5$) (the average noise rms for the antennas 1,4,5 and 6 is 7.6 mV, 4.8 mV, 12.6 mV and 6.4 mV respectively).

In order to follow the same analysis for both the simulation and experimental data the RF signals of the simulation sample were filtered in the frequency range 30-80 MHz (bellow 30 MHz the ionospheric noise increases while above 80 MHz strong signals from the radio FM band are expected). Finally in the simulation sample the event selection criteria described in [10, 16, 18] were imposed, which are based on the signal to noise ratio (SNR), the pulse rising time and the signal polarization. In brief we report that the cut values for the SNR, the rising time (RT) and the degree of polarization (p) are set to SNR$\geq$6, RT$\leq$28 ns and p$\geq$ 0.85 respectively. The final simulated sample consisted of 9180 events for the rest of the analysis.

The main goal of the present analysis includes the reconstruction of the shower axis direction using the data from the RF antennas. A sensible definition of the RF pulse arrival time is that it corresponds to the arrival time of the signal's maximum. However as indicated by previous studies [29] the time of the signal peak depends strongly on the system's characteristics, the background noise level and the filter characteristics. During the filtering process a Fast Fourier Transform (FFT) is applied and after removing the non-desirable frequencies the signal is transformed back to time domain with the inverse Fourier Transform (FFT^{-1}). Since the FFT breaks up the signal into complex exponentials the introduction of negative frequencies (with no physical mean) in the signal is inevitable. After transforming the signal to the time domain the effect of the neglected negative frequencies appears as a displacement of the position of the pulse maximum (due to the phase difference they cause). In order to eliminate this effect it is commonly used the analytical signal (or signal's envelope) instead of the signal itself. The analytic signal ($\hat{V}(t)$) is a complex function where the real part is the signal V(t) while the imaginary part is the Hilbert transform [4] $\mathcal{H}V(t)$. The Hilbert transform is used to withdraw the phase differences caused and restore the position of the pulse maximum (before filtering). For that reason, in order to eliminate the above dependencies, the arrival time can be defined as the time that the signal's envelope reaches its maximum value. The signal's enveloped is defined as

$$\hat{V}_{ew/ns}(t) = \sqrt{V^2_{ew/ns}(t) + (\mathcal{H}V_{ew/ns}(t))^2} \tag{1}$$

where $V_{ew/ns}(t)$ is the measured signal and $\mathcal{H}V_{ew/ns}(t)$ is its Hilbert transform. In figure 2 it is

[2] The convolution expresses how the shape of the impinging field is modified by the antenna characteristics.

[3] Antenna signals containing continuous recordings of the electromagnetic background of the area.

[4] The Hilbert transform of the signal $V(t)$ is defined as the convolution of $V(t)$ with the function $h(t) = (\pi t)^{-1}$, $\mathcal{H}V(t) = V(t) * \frac{1}{\pi t} = \frac{1}{\pi}\int_{-\infty}^{\infty} \frac{V(t)}{t-\tau} d\tau$

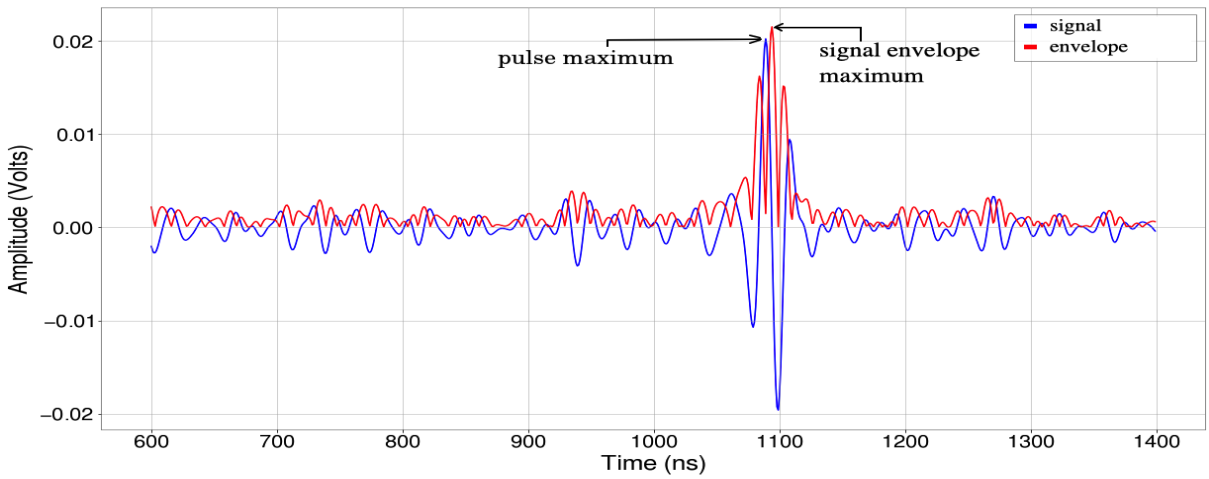

Figure 2. The recording EW signal timeseries (blue line) of an event and the corresponding signal envelope (red line).

shown the EW filtered RF waveform (blue line) for a cosmic event and the corresponding (red line) signal's envelope.

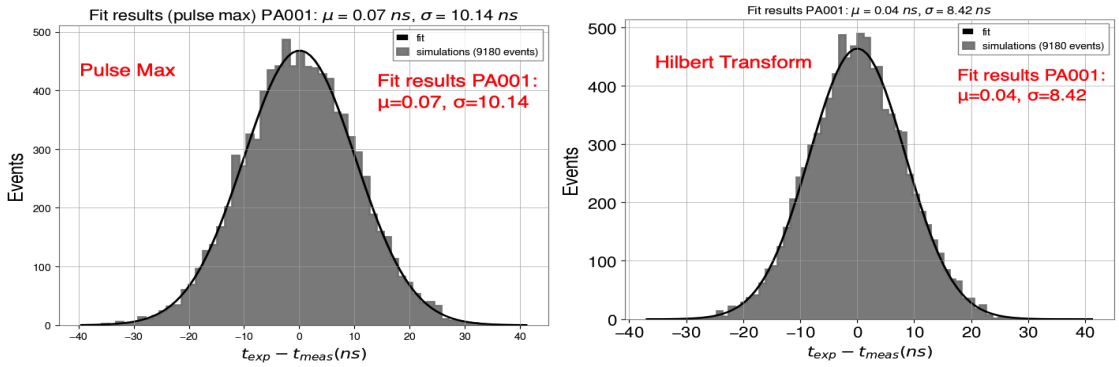

Figure 3. (*Left*) The distribution of the difference between the expected and the measured RF signal timing for the antenna 1. For the measured RF timing the position of the signal's maximum is used. (*Right*) The same distribution when the position of the envelope's maximum is used.

Recovering the 4 arrival time (t_i) of the pulses in the antennas and considering plane wavefront for the RF signal the calculation of the zenith (θ) and azimuth (ϕ) angles of the shower axis direction is done by minimizing the χ^2

$$\chi^2 = \sum_{i=1}^{4} \left(c(t_i - t_0) - (ux_i + vy_i)\right)^2, \quad u = \sin\theta\cos\phi, v = \sin\theta\sin\phi \tag{2}$$

where x_i, y_i are the positions of the antennas in the station coordinate system while t_0 corresponds to the time that the shower plane arrives in the origin of the station's coordinate system. In order to quantify the effect of using the time of the maximum in the envelope instead of the time of the signal maximum, in reconstructing the axis direction a large simulation sample was used.

Table 1. The sigma values for the distributions of the differences t_{exp}-t_{meas} for antenna 1,4,5,6.

	Antenna 1	Antenna 4	Antenna 5	Antenna 6
σ (pulse max)(ns)	10.1	10.4	10.2	10.4
σ (envelope max)(ns)	8.4	8.9	8.5	8.8

Using the true axis direction from the simulations and taking into account the positions of the RF antennas in the local coordinate system of the station, the timing of the RF signal (t_{exp}) can be estimated assuming plane shower front. Furthermore the timing of the pulse (t_{meas}) was calculated using both the signal's and the envelope's maximum. The resulting distributions of the differences t_{exp}-t_{meas} for the case of the signal's and the envelope's maximum, for antenna 1, are shown in figure 3 (left and right respectively). In both cases the distributions are fitted with Gaussians functions with mean value near zero and sigma at around 10.14 ns when using the signal's maximum and approximately 8.42 ns when using the envelope's maximum. The sigma values for the distributions of the remaining antennas are shown in table 1. As expected the RF timing is more accurate using the time of the maximum in the signal's envelope. Consequently, for the rest of the analysis the shower axis reconstruction is made using the timing of the peak in the signal's envelope.

In order to examine the sensitivity of the RF signal timing on estimating the shower axis direction, the method was applied to a large sample of the simulation events. In figure 4 is depicted the distributions of the difference between the true and the estimated, zenith ($\theta_{true} - \theta_{RF}$) and azimuth ($\phi_{true} - \phi_{RF}$) angles. Both distributions are fitted with Gaussians functions with mean around zero and sigma equal to 2.21^0 for the zenith and 4.95^0 for azimuth. In the right plot is shown the distribution of the angle between the true shower direction and the reconstructed direction using the RF timing data (3-d angle). The median of this distribution is 2.43^0.

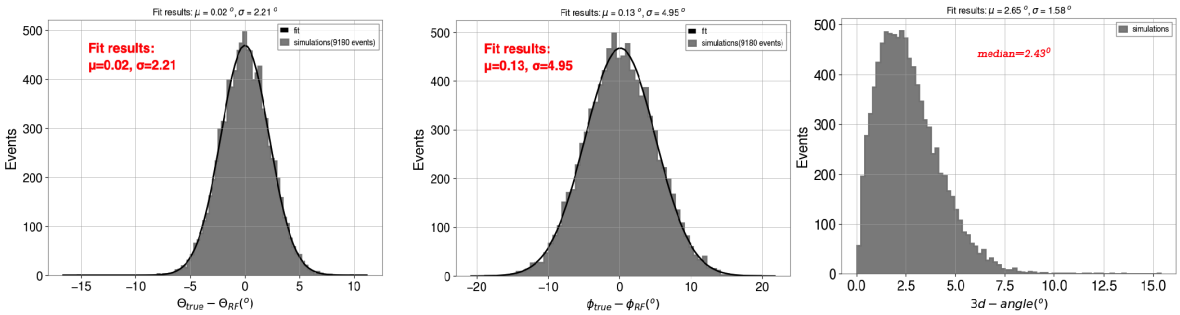

Figure 4. The distributions of the difference between the true and estimated, zenith (left) and azimuth (middle) angles. Both distributions are fitted with Gaussians functions with mean around zero and sigma equal to 2.21^0 for the zenith and 4.95^0 for the azimuth. In the right plot is shown the distribution of the angle between the true shower direction and the reconstructed direction using the RF timing data (3-d angle). The median of this distribution is 2.43^0.

The next step in the analysis includes the study of the dependence of the angular resolution of the RF timing method on the direction of the EAS and the RF signal amplitude. In figure 5 is depicted the resolution in estimating the zenith angle (black stars), the azimuth angle (blue circles) and the median of the 3d-angle (red boxes), as a function of the zenith (left), the azimuth (middle) and the amplitudes of the RF signal (right).

The zenith angle resolution worsens, as the zenith angle of the primary nuclei gets larger.

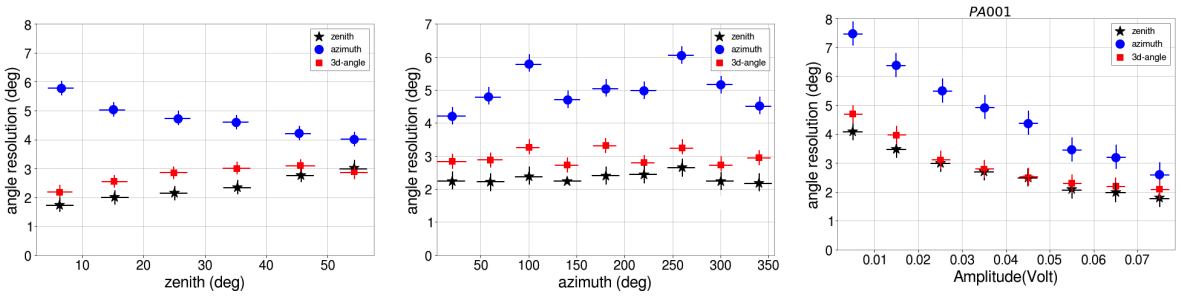

Figure 5. The zenith (black stars), the azimuth (blue circles) and the 3d-angle (red squares) resolution versus the zenith (left), the azimuth (middle) and the RF signal amplitudes (right) as evaluated from simulation. The resolutions are evaluated as the sigmas of the Gaussian functions that fit the distributions of $\theta_{true} - \theta_{RF}$ and $\phi_{true} - \phi_{RF}$ while for the 3d-angle resolution the median of the corresponding distribution is used.

Such dependence is expected since the antenna response (as described in [10]) is reduced for large zenith angles. Inclined showers will induce weaker signals on the antennas, relative to the signals induced by vertical showers. The resolution in estimating the azimuth angle is expected to improves as the zenith angle increases (inverse proportional to $\sin\theta$) which is evident from the simulation analysis. The resolution in estimating the zenith angle is approximately constant with respect to azimuth angles while the corresponding resolution in estimating the azimuth appears larger near 90^0 and 270^0 due to the small response of the antennas at these azimuth angles as well as the small RF amplitudes expected due to the dominant geomagnetic mechanism. Finally the resolution of both the zenith and azimuth angle become better as the pulse amplitudes increase resulting to a clean signal far above the background.

4. Data Analysis

The sample of data used in the present work was collected by the 3SDM-4RF [22] station and corresponds to about 25,900 hours of operation time. The data sample consisted of approximately 480,000 showers detected and successfully reconstructed by the station's SDM. Of these events, those exhibited RF signals above the background noise level to all 4 antennas were estimated to be 3800. After assuming the same event selection criteria as described for the simulations our final data sample consisted of 920 events.

In figure 6 is depicted the distribution of the RF signal amplitudes for each antenna of the station, for experimental data (black stars) and simulations estimation (histogram), normalized to the operation time of the station. The corresponding distributions for the measured RF amplitudes are in very good agreement with the simulations predictions. Furthermore it is evident that the distributions for the two distant antennas (4 and 6) are shifted to smaller values as expected for shower cores near the station's center. Figure 7 presents the distributions of the zenith (left) and azimuth (right) angles of the reconstructed shower axis direction. The experimental data are represented with black stars, while the simulations prediction with histograms. The corresponding agreement between data and simulations predictions is evident.

As explained before the dominant mechanism for the RF signal emission comes from the geomagnetic field. Consequently the amplitude of the RF signal is proportional to $\sin\alpha$, where α is the geomagnetic angle, ie. the angle between the EAS axis direction and the geomagnetic field. In figure 8 is presented the zenith and azimuth angles of experimental data (black stars) as reconstructed using the RF signal timing while the color contours represent the values of $\sin\alpha$. As it is expected less events are detected from directions with small values of $\sin\alpha$ indicating

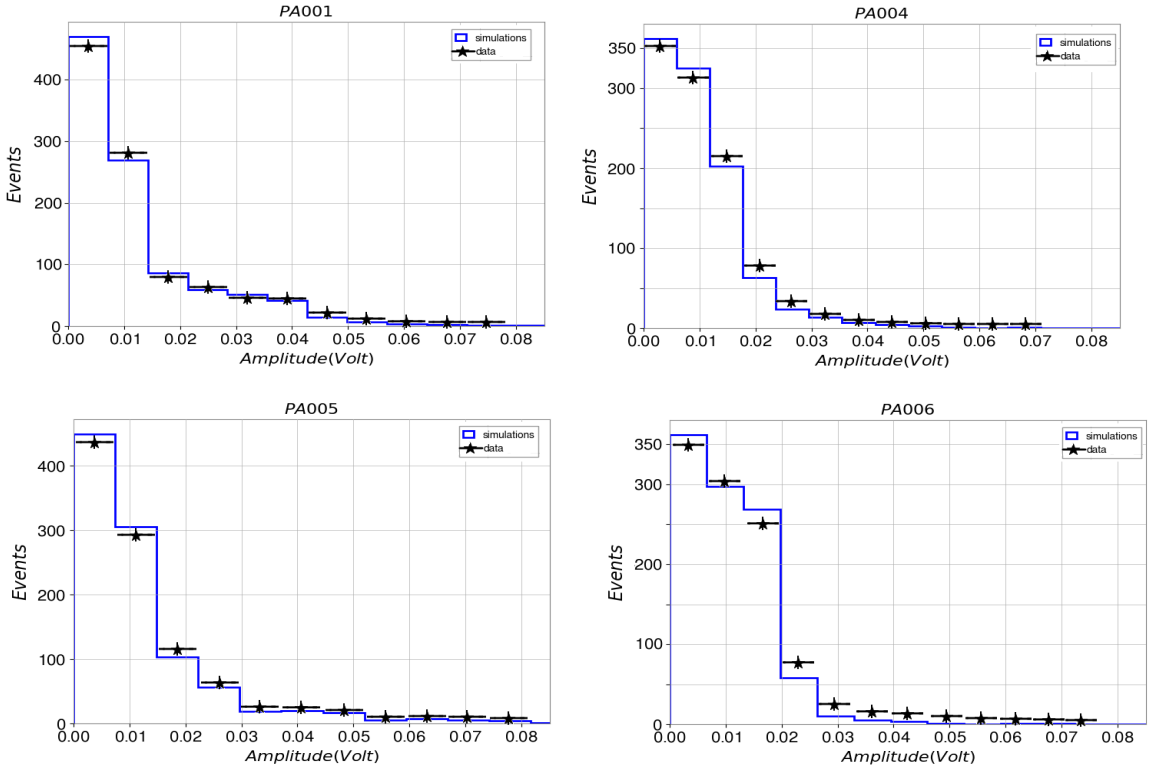

Figure 6. The distributions of the pulses amplitudes for the 4 antennas of station A, for experimental data (black stars) and simulations (histograms).

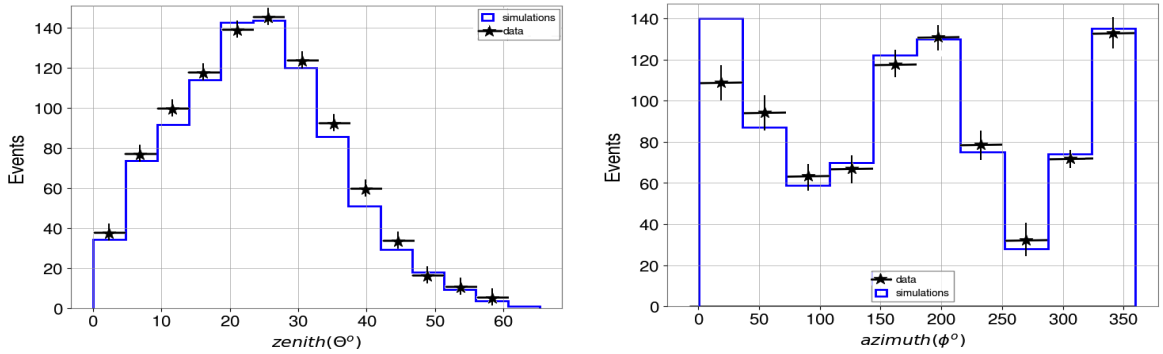

Figure 7. The distributions of the zenith (left) and azimuth (right) angles of the reconstructed shower axis direction. The experimental data are represented with black stars, while the simulations prediction with the histogram.

that the data sample is compatible with the geomagnetic mechanism.

5. Correlation of RF and SDM data

An independent shower axis reconstruction is performed using the timing information from the station's SDM. In figure 9 is depicted the distributions of the zenith (left) and azimuth (right) angles as calculated using the SDM timing data (black stars) and the RF timing data

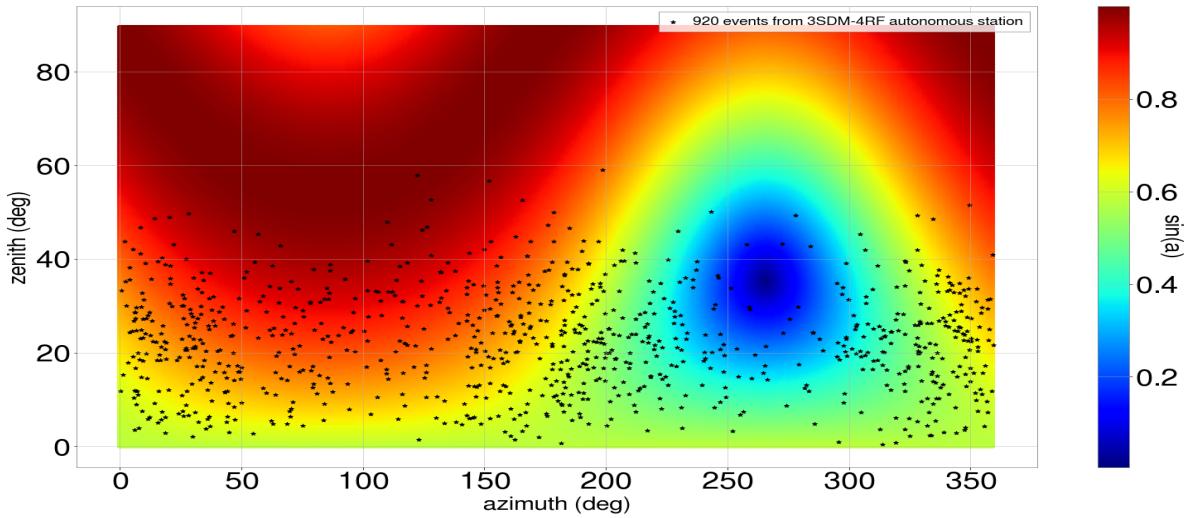

Figure 8. The zenith and azimuth angle for the experimental events as reconstructed using the RF signal timing (black stars). The color contours are associated with the values of the geomagnetic angle as a function of the two angles.

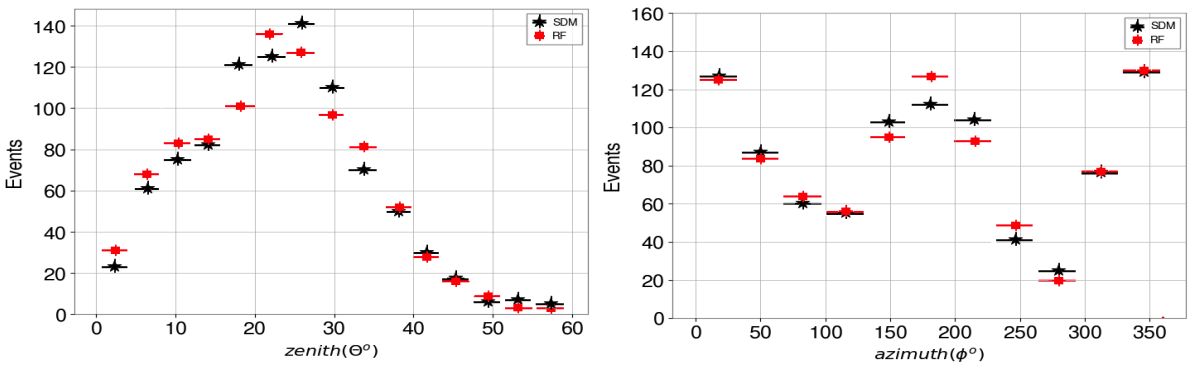

Figure 9. The distributions of the zenith (left) and azimuth (right) angles as calculated using the timing data from the SDM (black stars) and the RF (red circles).

(red circles). The distributions show that the direction estimated with the RF system is highly correlated with the direction estimated from the SDM data. In figure 10 (left) is shown the distribution of the difference between the estimated zenith angle using the SDMs data and the RF data (red points) while the histogram corresponds to simulations predictions. The same distribution for the azimuth angle is shown in the middle plot. Both distributions are fitted with Gaussians functions with mean around zero and sigma equal to 3.15 ^{0} for the zenith and 6.63 ^{0} for azimuth. In the right plot of figure 10 is shown the distribution of the 3d-angle as estimated using the SDM and the RF timing data. The median of this distribution is 3.27 ^{0}. In all cases the sigmas of the distributions are compatible with the individual resolutions of the SDM system [5] and the RF system (fig 4), which means that the sigmas are the quadratic sum of the resolutions achieved by the two systems.

[5] The corresponding zenith and azimuth resolution is $\sigma_{\Delta\theta} = 2.4^0$, $\sigma_{\Delta\phi} = 4.6^0$

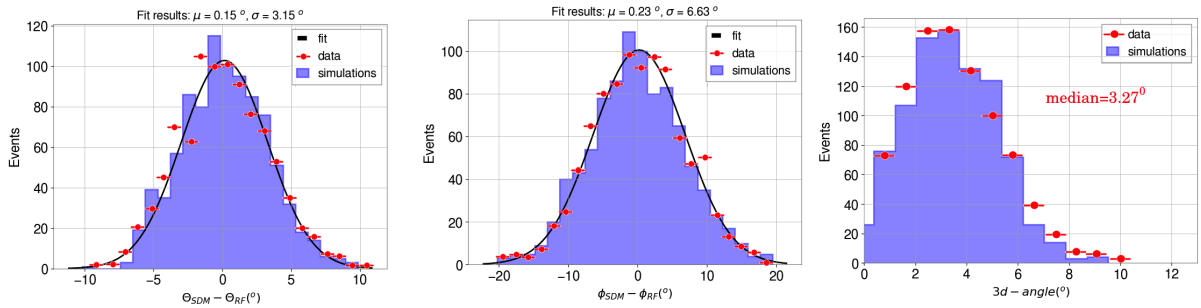

Figure 10. The distributions of the difference $\theta_{SDM} - \theta_{RF}$ (left) and $\phi_{SDM} - \phi_{RF}$ (middle). The distribution of the 3d-angle (right) as estimated using the SDM and the RF timing data. In all plots the red points correspond to experimental data while the histogram to simulation predictions.

6. Conclusions

We have presented a study in which the reconstruction of the shower axis direction was carried out using the timing information from the RF antennas of an Astroneu station. We used a sample of 920 shower events collected by the 3SDM-4RF [22] station of the Astroneu array where 4 RF antennas are triggered when a shower event is detected by the 3 SDMs of the station. The same analysis was performed using a sample of 9180 very high energy simulation events. The good agreement between RF data and simulations as well as between SDM data and RF data indicates that the RF signal from high energy induced air showers can be isolated efficiently even from small scale hybrid stations operating in areas with strong electromagnetic background.

Acknowledgments

This research was funded by the Hellenic Open University Grant No. ΦΚ 228: "Development of technological applications and experimental methods in Particle and Astroparticle Physics"

References

[1] J. V. Jelley et al. 1965 *Nature* **205** 327
[2] H. Falcke et al. - LOPES collaboration 2005 *Nature* **435** 313-316
[3] L. Martin et al. Proc.35th ICRC (2017)
[4] P. Schellart et al. 2015 *Astron. Astrophys.* **66** 31
[5] The Pierre Auger Coll. 2016 *Phys. Rev. D* **93** 122
[6] W.D. Apel et al. 2016 *Phys. Lett. B* **763** 179
[7] R. Dallier. 2015, *PoS (ICRC2015)* **293**
[8] B. Revenu et al. 2017, *PoS (ICRC2017)* **416**
[9] C. Welling et al. 2019 *JCAP10* **2019** 075
[10] S Nonis et al. 2020 *Phys. Scr.* **95** 084007
[11] A. Muniz et al., 2020, *Sci. China Phys. Mech. Astron.* **63** 219501
[12] O. Scholten, K. Werner, F. Rusydi 2008 *Astropart.Phys.* **29** 94-103
[13] G.A.Askaryan 1962 *Phys. JETP* **14** 441
[14] T. Avgitas et al. 2020 *JINST* **15** T03003
[15] S.E. Tzamarias et al. 2021 *Instrum Exp Tech* **64** 127-140
[16] I. Manthos et al., 2020, *New Astronomy* **81** 101443
[17] A. Leisos et al. 2019 *Universe* **5** 3
[18] S. Nonis et al. 2019 *EPJ Web of Conferences* **210** 05010
[19] D. Charrier, 2012 *Nucl. Instrum. Methods Phys. Res., Sect. A* **662** 142-145
[20] A. Leisos et al, Performance of the autonomous stations of the Astroneu extensive air shower array, arXiv:1801.04768
[21] A. Leisos et al, 2021 *New Astronomy* **82** 101448
[22] A.G. Tsirigotis et al, 2020 *Eng. Res. Express* **2** 025027
[23] S. Hansen et al. 2004 *IEEE Transactions on Nuclear Science* **51** 926-930
[24] D. Heck et al. 1998 *Forschungszentrum Karlsruhe Report* **FZKA** 6019
[25] T. Gaisser et al. 2013 *Front. Phys.* **8** 748-758
[26] S. Ostapchenko 2011 *Phys. Rev. D* **83** 014018
[27] H. Fesefeldt 1985 *Report PITHA* **85** 02
[28] V. Marin et al 2012 *Astropart. Phys.* **35** 733
[29] P. Schellart et al. 2013, *A&A*, **560** A98